3B2v8.06a/w (Dec 5 2003).51c XML:ver:5.0.1 JQSRT : 2203 Prod.Type:FTP pp.1–20(col.fig.:NIL) ED:Prathiba PAGN:vs SCAN:Mouli

ARTICLE IN PRESS

ELSEVIER

Journal of Quantitative Spectroscopy & Radiative Transfer ▮ (▮▮▮▮) ▮▮▮–▮▮▮

Journal of Quantitative Spectroscopy & Radiative Transfer

www.elsevier.com/locate/jqsrt

Collisional parameters of H_2O lines: effect of temperature

G. Wagner[a], M. Birk[a], R.R. Gamache[b], J.-M. Hartmann[c,*]

[a]*Institute for Remote Sensing Technology, German Aerospace Center (DLR), Münchner Str. 20, D-82234 Wessling, Germany*

[b]*Department of Environmental, Earth, and Atmospheric Sciences, University of Massachusetts Lowell, 265 Riverside Street, Lowell, MA 01854, USA*

[c]*Laboratoire de Photophysique Moléculaire, Université Paris-sud, Bât. 350, 91405 Orsay Cedex, France*

Received 12 February 2004; accepted 30 July 2004

Abstract

High-resolution Fourier transform spectra of H_2O–air mixtures have been measured at 296, 742, and 980 K for total pressures of 0.5 and 1.0 atm in the region of the ν_2 band. From these recordings, air-broadening coefficients have been determined for the doublet lines with $K_c = J$. From these data and previous experimental determinations, line-broadening parameters $\gamma(T)$ are obtained at all three temperatures for the doublet lines from $J = 0$ up to 16. These values are then used to deduce the temperature-dependence exponent n such that $\gamma(T) = \gamma(296) \times (296/T)^n$. The values of n obtained using the two elevated temperatures are consistent and show that line widths decrease with T for small J-values ($n \approx +0.8$), are almost temperature independent on T for $J \approx 10$, and increase with T for high J lines ($n \approx -0.3$ for $J \approx 15$). This original result, which confirms theoretical predictions made about 15 years ago with a semi-classical approach (J. Chem. Phys. 86 (1987) 144), is analyzed here using an improved version of the model. Comparisons between measured and computed widths show that calculations cannot correctly reproduce the experimental results at all temperatures simultaneously. This failure is attributed to the use of an inappropriate interaction potential and to the very strong dependence of the broadening $\gamma(v)$ on the relative velocity v for high J lines. This strong variation of $\gamma(v)$ raises the question (which is discussed here) what calculated quantity is to be compared with measured values (i.e. $\gamma[\bar{v}(T)]$, $\overline{[\gamma(v)]}\,(T)$, or some other more complex mean to account for the velocity averaging of the spectral profile itself?). Nevertheless, when

*Corresponding author. Tel.: +33-1-69-15-75-14; fax: +33-1-69-15-75-30.
E-mail address: jean-michel.hartmann@ppm.u-psud.fr (J.-M. Hartmann).

0022-4073/$ - see front matter
doi:10.1016/j.jqsrt.2004.07.023

the temperature exponent n is considered, satisfactory agreement between experiments and predictions is obtained, particularly when the averaging of widths over the relative velocity distribution is made.

Keywords: ■; ■; ■

1. Introduction

Because of the important role played by water vapor in thermo-physical processes in our atmosphere and combustion media, knowledge of the temporal and spatial variations of the distributions of H_2O is essential. Hence, the need for precise remote sensing has stimulated numerous studies of the spectroscopic parameters of H_2O lines. Among these, the air (or N_2 and O_2) broadening and shifting parameters have received considerable experimental attention ([1–3] and references therein). Nevertheless, while there have been many determinations of Lorentz widths γ at room temperature, their variations with T have been much less studied. Analysis of the available measurements [3] shows that, for the ν_2 band, there are more than 3000 determinations of air- or N_2 broadening near 296 K, but that the effects of temperature have been investigated less than 300 times. The reasons for this are the strong decrease of H_2O saturation pressure at low T and the fact that most experimental setups either do not permit variable temperature or are designed for cooling. In most temperature-dependent studies, the range is typically 250–300 K (e.g. [4]), and this restriction has two main consequences. The first is that transitions between levels of high rotational energy are not investigated. Lines with $K_c = J$, for instance, have been measured up to $J \approx 16$ at 296 K, but the effects of temperature have only been investigated for $J \leqslant 8$. The second consequence is that the uncertainty on the temperature-dependence parameter n, such that $\gamma(T) = \gamma(T_0) \times (T_0/T)^n$, is quite large [1] since $\gamma(T)/\gamma(T_0)$ and (T_0/T) are close to unity due to the limited temperature range. Hence, the available measurements of n do not permit a severe test of theoretical models since: (i) the uncertainties on n are large; and (ii) the measurements are limited to transitions of relatively low rotational quantum numbers J for which the temperature exponents n are practically all close to the values of 0.83 and 0.75 associated with resonant dipole–quadrupole and quadrupole–quadrupole interactions, respectively. Studies at elevated temperature, which are unfortunately very few due to experimental difficulties, are interesting since they provide more precision on n and enable investigation of thetemperature dependence for transitions covering wide ranges of J-values. Indeed, theoretical calculations made a while ago [5] have predicted that n may show large variations from line-to-line and could even be negative for transitions (of high rotational energy) which involve very non-resonant collisions. This interesting and still unconfirmed result, together with the ability of the theoretical approach of Ref. [2,6,7] predict the temperature dependence of air-broadened H_2O widths, is the subject of the present work.

In this paper, the air broadening of $K_c = J$ doublets (i.e. $J \pm 1_{0,J\pm1} \leftarrow J_{1,J}$ and $J \pm 1_{1,J\pm1} \leftarrow J_{0,J}$) of the ν_2 band of water vapor is considered. These particular transitions are interesting since they involve rotational energies rapidly increasing with J. Hence, collisions quickly become very non-resonant leading to a number of effects. (a) The first is the rapid decrease of the widths from typically 0.1 cm^{-1}/atm for small J-values down to more than 10 times less for $J \approx 15$ at room

temperature [2]; (b) due to the small rotational contribution to the widths for high J lines, the vibrational dependence of the intermolecular potential can have significant effects leading, as demonstrated in Ref. [2], to variations of the widths with the vibrational band; (c) collision-induced rotational transfers for high J lines being very non-resonant, widths independent on T or even increasing with T are expected due to a *resonance overtaking* mechanism [5]; (d) for the same reason, the broadening parameters should depend strongly on the relative velocity of the collisions. Hence, deviations from usual line shapes due to inhomogeneous effects resulting from velocity averaging are expected [8,9]. The first two points, (a) and (b), have been addressed and analyzed in Ref. [2], (d) will be the subject of a future paper,[1] and the present work is devoted to (c).

High-resolution Fourier transform spectra of H_2O-air mixtures have been recorded at DLR for temperatures 296, 742 and 980 K and total pressures 0.5 and 1 atm. These measurements were made within the frame of two EC projects for non-intrusive measurement of aircraft engine exhaust emissions [10–12]. From these spectra, air-broadened widths have been deduced for a number of transitions among which we have selected the $K_c = J$ doublets of the ν_2 band which have been studied up to $J \approx 12$ at room temperature and over $J = 18$ at higher temperatures. Comparisons between the present 296 K determinations and previous measurements demonstrate the consistency of various experimental results. Using all available room temperature values, a set of air-broadened widths is then constructed for the doublet lines for rotational quantum numbers J ranging from 1 to 16. These values are used, together with the measurements at 742 and 980 K, to deduce two sets of temperature exponents n. The latter are consistent and confirm the predictions of Ref. [5], since n varies from $+0.8$ for low J lines down to about -0.3 for high J transitions. Theoretical calculations are also made using the model of Refs. [2,6,7]. They quantitatively reproduce the measured temperature exponents although the widths themselves are overestimated for high J lines. These results are discussed in terms of the intermolecular potential at short distances and of the strong dependence of broadening cross sections on the relative velocity.

The remainder of this paper is divided into three sections. The experimental details and procedures for the treatment of measured spectra are described in Section 2. The measured half-widths are given and compared with previous measurements in Section 3, where temperature exponents and the procedure used to determine them are presented. Finally, theoretical predictions and their comparisons with experimental determinations are given in Section 4.

2. Experimental details

Spectrometer setup: Measurements were carried out in absorption with a Bruker IFS 120 HR Fourier transform spectrometer in the spectral range 1550–2300 cm^{-1} applying a Globar source, Ge/KBr beamsplitter, and MCT ($<1800\,cm^{-1}$) and InSb ($>1800\,cm^{-1}$) detectors in combination with suitable optical filters. The unapodized resolution was 0.01 cm^{-1} (maximum optical path difference 50 cm). Radiometric accuracy was checked, especially detector non-linearities combined

[1] A study of N_2 broadened low, medium, and high $JK_c = J$ doublets of H_2O in the ν_3 band at room temperature is in progress and will be the subject of a forthcoming paper.

with phase errors and the effect of thermal radiation of the cell windows and sample were investigated and corrected. The instrument was properly aligned and the instrumental line shape measured utilizing the residual water apparent even at 10^{-2} mbar in the spectrometer. The measurement time of individual spectra was between 2 and 10 min. Reference spectra were taken prior and after a series of measurements with the same resolution as in sample measurements. Source off spectra was taken in case of elevated cell temperatures and subtracted from the source on spectra to remove the sample and cell window thermal emission. Finally, unapodized transmittance spectra were formed for further data reduction.

Absorption cell: A new design for a high-temperature cell (up to 1000 K) has been elaborated during the EC Aerojet project [10] to be used inside the evacuated sample compartment of the spectrometer. The cell body is made of fused silica and heated electrically. Its absorption path length is about 16 cm and its diameter 4 cm. Calcium fluoride was selected as window material to cover the spectral ranges of interest. The windows are equipped with radiative heating in order to decrease temperature inhomogeneities. The cell features a heatable gas inlet and an outlet to allow measurements with a gas flow while maintaining a homogeneous gas temperature over the cell volume. The cell features radiation shields and is mounted inside a water-cooled vacuum-tight housing for thermal insulation equipped with two additional calcium fluoride windows. The temperature of the cell body is measured with two Pt100 thermo resistors applying a Lakeshore DRC-93C temperature controller and DIN 43760 calibration curves.

Temperature determination: A very crucial point is the determination of the average gas temperature. CO was measured under the same conditions as the water/air mixture. From a least-squares fit of the retrieved line strengths the average gas temperature could be determined. A polynomial relation between temperature sensor readings and average gas temperature was established. Temperature errors ranged between 0.5 K at ambient and 1.5 at 1000 K.

The gas-handling system: All parts in contact with the sample gas are made of Duran glass, stainless steel or PTFE. A cold trap allows to freeze out the water for purification purposes. Mixtures are prepared in a stainless-steel mixing chamber (volume ca. 4 l) equipped with a magnetic stirrer. Pressures are measured with 10, 100, and 5000 mbar type 127A MKS Baratrons. The mixing chamber also serves as a gas reservoir for the flow measurements. The system is equipped with two vacuum pumps for evacuating system and cell as well as for maintaining the gas flow during the measurement. The flow rate was set by a needle valve downstream from the cell. The cell pressure was measured with a 1000 mbar range MKS Baratron type 127A and was kept constant by an upstream electronically controlled valve (MKS type 248AC) in combination with a MKS PI controller type 1250B. The settings for the needle valve were calibrated with a MKS mass flow controller type 1259C. Pressure uncertainties were smaller than 0.35%

Preparation of gas mixtures: Water vapor was filled into the mixing chamber up to the desired pressure (2–10 mbar). The mixing chamber was closed and the gas-handling system evacuated. The mixing chamber was then filled with air to about 2 atm. Special care was taken to maintain an air pressure higher than or equal to the pressure in the chamber in order to avoid any backflow of gas into the handling system. The gas was allowed for a short time for thermal equilibration before taking the final pressure readings. Five minutes of stirring was found sufficient to ensure complete homogeneity of the mixture.

Time constant for wall conditioning of tubing and hot cell: In order to have a defined water partial pressure in the cell a steady flow has to be applied. This is due to the tendency of water to stick to

the walls of cell and tubing. Although the effects of wall conditioning are less dramatic under flow conditions it had to be verified that the composition of the gas mixture remains unchanged when transported from the mixing chamber through the tubings and through the cell. This was done by spectroscopic monitoring of the sample gas. The integral opacity under a part of the absorption band was measured. A flow speed of 50 standard-cm^3/mn was applied to allow complete exchange of the cell contents every 4 min at 300 K. The water signal was found to increase after starting the flow for about 30 min before staying constant. Stopping the flow or changing the flow speed barely affected the results. Unfortunately, the mixing chamber was down to ambient pressure after this time and a quick refill was necessary. After starting the flow again steady state was reached after another 10 min with about 30 min of measurement time left.

Measurements: For the present work only a part of the available measurements were used: at 296 K: 0.5,1 atm; at 743 K: 0.5,1 atm; at 977 K: 1 atm; at 981 K: 0.5 atm. The water volume mixing ratio was about 0.5% for all measurements.

Analysis: The line parameter analysis was performed with the FitMAS software [13]. Microwindows were selected to obtain isolated groups of lines which are fitted simultaneously. As line model the monochromatic Voigt transmittance line shape was convolved with the instrumental line-shape function. The line position, line strength and Lorentz half-width were fitted simultaneously with a quadratic polynomial baseline. Fig. 1 gives an example of a microwindow fit for a high J line. As can be seen around the center of the narrow line near 1979 cm^{-1}, residuals significantly deviate from noise. As observed previously [8,9], the largest discrepancies are observed for high J lines with small pressure broadened half-width and thus a larger contribution of the Doppler profile to the overall line shape. Applying an uncorrelated

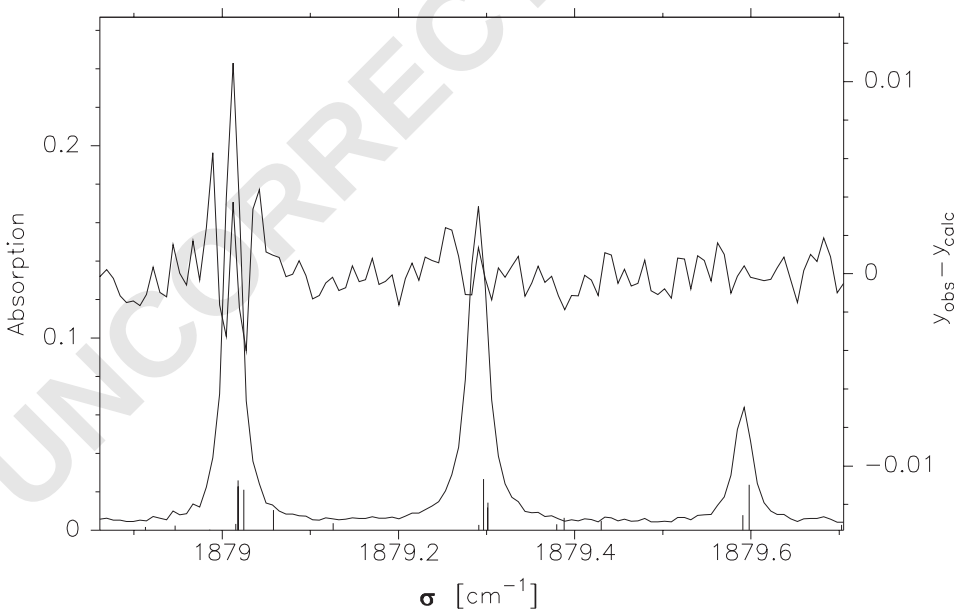

Fig. 1. Exemplary microwindow fit result of a 980 K, 0.5 atm spectrum, applying a Voigt line profile. Lower trace: measured spectrum, upper trace: (observed-calculated) ×10, bottom: logarithmic stick plot of line-strengths.

Table 1
Inter-comparison of fitted pressure-broadened half-widths of selected transitions in spectra recorded around 980 K with 0.5 atm and 1 atm total pressure, applying a Voigt or an uncorrelated Rautian line profile

Transition $J_f, K_{a_f}, K_{c_f} - J_i, K_{a_i}, K_{c_i}$	γ (cm^{-1} atm^{-1}) Voigt profile		γ (cm^{-1} atm^{-1}) Uncorrelated Rautian profile	
	0.5 atm	1 atm	0.5 atm	1 atm
4,1,4–3,0,3	0.0405(4)	0.0392(2)	0.0412(4)	0.0395(2)
15,0,15–14,1,14 15,1,15–14,0,14	0.0116(1)	0.0116(1)	0.0130(1)	0.0121(1)
16,0,16–15,1,15 16,1,16–15,0,15	0.0102(1)	0.0102(1)	0.0123(1)	0.0110(1)

Transitions are labeled with index i for initial and f for final state. 1σ statistical uncertainties in units of the last given digit are given in parentheses.

Rautian profile taking into account collisional narrowing considerably decreases these residuals. In Table 1, air-broadening parameters from measurements at 0.5 and 1 atm total pressure and 980 K are given for the two line-shape models in case of one low J line (broad) and two high J lines (narrow). The resulting pressure-broadening parameters show significant changes for the high J lines for different models. For the case of 0.5 atm and 980 K the width is increased by 2%, 12%, 17% for $J_i = 3$, 14, 15, respectively and for the case of 1 atm and 980 K, 1%, 4%, 8%, respectively. The overall trend in these differences can be understood by the contribution of the Doppler width to the overall line profile which is larger at lower total pressure and increases with increasing J. Since the ratio of Doppler and pressure broadened half-width is different for 0.5 and 1 atm the intercomparison of the pressure broadened half-widths for different total pressures is a good test of the validity of the profile used. Surprisingly, the results obtained with the simple Voigt profile with bad residuals agreed extremely well within the statistical uncertainty, while the results for the uncorrelated Rautian profile show significant differences. For the Voigt profile the low J line results agree within 4σ and the high J lines within 1σ. For the Rautian profile the low J line results differ by 5σ and the high J line results differ by 9σ and 13σ. The rather inconsistent results for the low J line can be addressed by residual water signatures from different water amounts in the instrument in the sample and reference measurements. These results were verified by performing the same analysis for themeasurements at about 740 K. Despite the residuals, the results obtained with the Voigt profile are physically more meaningful and are thus used in the further analysis.

3. Experimental results

3.1. Half-widths

Starting from the half-widths extracted from the 0.5 and 1.0 atm spectra of the InSb and HgCdTe detectors, we have selected the doublet lines of the ν_2 band of $H_2\,^{16}O$ for which $K_c = J$.

These correspond to the transitions $J_{0,J} \leftarrow J-1_{1,J-1}$ and $J_{1,J} \leftarrow J-1_{0,J-1}$ and $J-1_{0,J-1} \leftarrow J_{1,J}$ and $J-1_{1,J-1} \leftarrow J_{0,J}$. The measured values obtained from the various spectra were then averaged at each temperature. Since the water vapor amounts in the studied H_2O–air mixtures is about 0.5% extracted widths need to be corrected for self-broadening. This was done using measured room temperature values for H_2O–H_2O from (mostly) Refs. [14,15] and, for 742 and 980 K, self-broadening temperature exponents were calculated using the model of Ref. [16]. While doing this, the uncertainty was determined from the scatter (maximum deviation) of the widths deduced from the various spectra around the average value.

This procedure gives, at room temperature, a set of air-broadening coefficients for m ($m = J_f$ and $-J_i$ for R and P lines, respectively) between -12 and 13. In order to check them, the databases of measured line-broadening coefficients [1,3], which contain all available measurements, were used. We selected, within the N_2- and air-broadened data, those for the specific transitions studied here ($K_c = J$ in the ν_2 band). Note, we have divided the N_2-broadened values by 1.09 in order to convert them to air broadening (tests using our databases indicate that this ratio, suggested in Ref. [17], is correct within ±2%). The resulting intercomparison of measurements, displayed in Table 2, shows a remarkable overall agreement. In particular, the present determinations (column a) agree with the average of previous ones (column b) within ±4% for almost all transitions with relative and absolute RMS deviations of 2.5% and $1.3 \times 10^{-3}\,\mathrm{cm^{-1}/atm}$. Then, in order to have a set of very reliable room temperature half-widths that extends to higher J-values and that are as precise as possible, we again used all the air- and N_2-broadening measurements (divided by 1.09) and we proceeded as follows. First, we selected all the measurements for the considered doublet lines and calculated the average value and RMS of the measured values for each of them. Using these mean values, we were able to check that the widths of the P and R transitions of identical (but reversed) rotational quantum numbers (e.g. $J_{0,J} \leftarrow J-1_{1,J-1}$ and $J-1_{1,J-1} \leftarrow J_{0,J}$) are identical within experimental errors. Note that theoretical calculations also indicate that the widths of these two transitions are extremely close to each other (as expected since differences between the energy structures in the ground and $\nu_2 = 1$ states are small). This shows that the widths of the considered lines only depend on $|m|$ ($m = J_f$ in the R branch and $-J_i$ in the P branch) and on K_a(= 0 or 1 for the transitions considered here). Hence, in order to extend the averaging of experiments for better precision, we calculated mean values and RMS of all measurements for the ν_2 doublet lines of identical $|m|$ and K_a. This leads to the room temperature values in column (a) of Table 3.

The 742 and 980 K measurements were treated the same way, i.e.: using the various measurements (0.5, 1 atm, HgCdTe and InSb), correcting them for self-broadening, and calculating averaged values and RMS also using the fact that permuting the upper and lower rotational quantum numbers does not change the half-widths. The results are given in columns (b) and (c) of Table 3 for the two elevated temperatures.

3.2. Temperature dependence

The broadening coefficients given in Table 3 are plotted in Fig. 2. They are qualitatively consistent with the predictions of Ref. [5] and confirm that the dependence on temperature strongly depends on the line. The broadening of low $|m|$ transitions decreases with T whereas it increases for high $|m|$ lines, the width being roughly independent on T for $|m| \approx 11$. From these

Table 2
Air-broadening coefficients ($10^{-3}\,cm^{-1}$/atm) at 296 K for $K_c = J$ lines of the $H_2\,^{16}O$ ν_2 band

J_f	K_{a_f}	K_{c_f}	J_i	K_{a_f}	K_{c_f}	(a)	(b)	(c)	(d)
11	0	11	12	1	12	14.6	14.8 (3)	14.9 0.9 [4] 14.2 0.3 [18]	15.3 0.8 [18]
11	1	11	12	0	12	14.6	14.4 (3)	14.7 0.9 [4] 14.0 0.8 [18]	14.6 1.1 [18]
10	0	10	11	1	11	21.1	19.7 (3)	19.9 0.8 [18] 18.7 1.1 [4]	20.6 0.7 [18]
10	1	10	11	0	11	20.4	20.3 (3)	19.7 0.6 [4] 20.7 0.4 [18]	20.7 0.3 [18]
9	0	9	10	1	10	26.3	27.3 (3)	26.7 0.8 [4] 27.4 0.6 [18]	27.8 0.3 [18]
9	1	9	10	0	10	26.2	27.2 (3)	28.0 0.8 [4] 27.5 0.2 [18]	27.8 0.5 [18]
8	0	8	9	1	9	34.5	36.0 (3)	36.3 0.5 [18] 35.2 1.1 [4]	36.6 1.1 [18]
8	1	8	9	0	9	34.8	35.2 (3)	35.3 1.1 [4] 34.7 0.7 [18]	35.8 0.7 [18]
7	0	7	8	1	8	46.2	46.7 (5)	46.11.4 [4] 45.8 0.2 [14] 46.2 0.3 [18]	47.6 1.9 [14] 47.9 0.5 [18]
7	1	7	8	0	8	46.0	46.6 (5)	46.2 0.8 [18] 46.6 1.4 [4] 47.1 0.8 [14]	47.2 1.8 [18] 46.1 4.2 [14]
6	0	6	7	1	7	59.2	60.7 (5)	57.8 0.6 [14] 59.4 0.8 [18] 59.8 1.8 [4]	65.0 1.2 [14] 61.5 0.6 [18]
6	1	6	7	0	7	57.7	59.8 (5)	58.0 1.7 [4] 58.7 0.3 [14] 59.5 1.2 [18]	61.7 0.6 [14] 61.0 0.8 [18]
5	0	5	6	1	6	73.6	74.7 (5)	73.7 2.2 [4] 73.7 0.2 [14] 72.5 1.0 [18]	77.2 1.0 [14] 76.4 0.6 [18]
5	1	5	6	0	6	70.0	71.1 (5)	69.4 2.1 [4] 71.7 0.4 [14] 69.8 0.6 [18]	72.5 0.9 [14] 72.5 1.4 [18]
4	0	4	5	1	5	86.0	87.1 (5)	85.5 1.5 [18] 84.9 2.5 [4] 86.1 0.3 [14]	89.9 2.8 [18] 89.4 1.4 [14]
4	1	4	5	0	5	81.7	83.5 (5)	84.0 0.6 [14] 81.2 1.4 [18] 81.0 2.4 [4]	88.1 0.6 [14] 83.1 1.1 [18]
3	0	3	4	1	4	93.8	95.4 (5)	91.5 1.0 [18] 93.9 2.8 [4] 95.5 0.3 [14]	95.5 0.7 [18] 101.0 1.0 [14]
3	1	3	4	0	4	89.7	90.8 (5)	89.5 4.0 [18] 89.6 2.7 [4] 89.8 0.2 [14]	91.5 0.5 [18] 93.9 1.8 [14]
2	0	2	3	1	3	97.3	99.1 (5)	98.3 0.8 [18] 97.7 2.9 [4] 97.4 0.3 [14]	100.0 1.0 [18] 102.0 1.6 [14]
2	1	2	3	0	3	96.4	98.5 (5)	96.1 2.9 [4] 97.1 1.5 [18] 98.6 0.1 [14]	99.3 1.4 [18] 102.0 0.8 [14]
1	1	1	2	0	2	101.0	103.0 (5)	101.0 0.8 [18] 99.9 3.0 [4] 104.0 0.8 [14]	102.0 0.8 [18] 106.0 3.3 [14]
0	0	0	1	1	1	101.0	99.2 (6)	101.0 2.5 [18] 101.0 3.0 [4] 95.0 9.5 [19] 99.1 0.2 [14]	102.0 5.5 [18] 97.4 5.0 [14]
1	1	1	0	0	0	100.0	100.0 (6)	94.0 9.4 [19] 99.8 0.5 [14] 102.0 3.0 [18] 100.0 3.0 [4]	103.0 1.2 [14] 103.0 1.8 [18]
2	0	2	1	1	1	101.0	102.0 (5)	100.0 1.5 [18] 99.6 3.0 [4] 102.0 0.5[14]	103.0 3.2 [18] 105.0 2.1 [14]
2	1	2	1	0	1	102.0	106.0 (5)	108.0 0.3 [14] 99.5 2.5 [18] 103.0 3.1 [4]	113.0 1.7 [14] 108.0 4.1 [18]

1	3	5	7	9	11	13	15	17	19	21	23	25	27	29	31	33	35	37	39	41	43
3	0	3	2	1	2	94.4	96.0 (3)	94.8 2.0 [18]	94.8 2.8 [4]												
3	1	3	2	0	2	97.4	99.7 (5)	99.0 1.5 [18]	97.4 2.9 [4]	99.5 0.6 [14]											
4	0	4	3	1	3	89.0	90.8 (5)	89.3 1.0 [18]	88.5 2.6 [4]	90.3 0.2 [14]											
4	1	4	3	0	3	93.7	97.4 (5)	92.8 2.8 [4]	99.4 0.3 [14]	94.0 5.0 [18]											
5	0	5	4	1	4	81.2	84.1 (5)	79.4 2.4 [4]	79.5 2.0 [18]	87.2 0.2 [14]											
5	1	5	4	0	4	85.0	87.7 (5)	83.8 2.5 [4]	87.7 0.3 [14]	86.5 2.0 [18]											
6	0	6	5	1	5	70.1	71.5 (5)	69.3 2.1 [4]	70.8 1.5 [18]	70.7 0.3 [14]											
6	1	6	5	0	5	74.8	76.3 (5)	72.9 2.2 [4]	78.3 0.3 [14]	72.7 2.0 [18]											
7	0	7	6	1	6	59.0	57.0 (3)	56.0 2.0 [18]	58.2 1.8 [4]												
7	1	7	6	0	6	61.0	61.6 (3)	60.5 1.8 [4]	61.5 1.5 [18]												
8	0	8	7	1	7	47.1	47.6 (3)	46.3 2.0 [18]	45.7 1.4 [4]												
8	1	8	7	0	7	47.8	47.8 (3)	47.5 1.0 [18]	46.6 1.4 [4]												
9	0	9	8	1	8	37.5	36.8 (3)	37.0 1.2 [18]	36.2 1.1 [4]												
9	1	9	8	0	8	36.3	36.6 (3)	36.5 1.0 [18]	35.9 1.1 [4]												
10	0	10	9	1	9	27.9	27.8 (3)	28.5 1.5 [18]	26.6 0.8 [4]												
10	1	10	9	0	9	27.4	27.7 (3)	27.9 1.3 [18]	27.7 0.8 [4]												
11	0	11	10	1	10	20.6	21.6 (3)	22.0 1.0 [18]	20.9 0.6 [4]												
11	1	11	10	0	10	20.2	21.7 (3)	22.0 2.5 [18]	21.3 0.6 [4]												
12	0	12	11	1	11	16.1	15.1 (3)	15.2 0.5 [4]	15.2 0.9 [18]												
12	1	12	11	0	11	16.1	15.7 (3)	15.4 0.4 [18]	15.4 0.5 [4]												
13	0	13	12	1	12	12.1	12.6 (4)	12.4 0.5 [18]	12.7 0.1 [20]	12.5 0.4 [4]											

Columns are the following: 1–6: rotational quantum numbers of the transition. (a) Present measurements. (b) Average value of the half-widths in columns (c) and (d) and, between parentheses, the number of values used for the average. (c) Air-broadened half-widths from the literature and, for each of them, the half-width, the uncertainty, the reference. (d) Same as (c) but the values are N_2 broadenings divided by 1.09.

Table 3
Air-broadened half-widths and temperature dependences

$\|m\|$	k_0	(a)	(b)	(c)	(d)	(e)
1	1	99.8 3.0 (12)	50.0 2.5 (4)	44.2 6.6 (2)	0.755 0.087	0.682 0.151
2	0	102.0 2.3 (10)	48.8 0.9 (4)	44.0 6.7 (2)	0.805 0.045	0.704 0.147
2	1	105.0 5.1 (8)	49.4 0.6 (2)	42.3 2.8 (2)	0.823 0.066	0.761 0.095
3	0	97.6 2.3 (8)	45.8 0.9 (4)	38.3 1.2 (2)	0.826 0.047	0.783 0.046
3	1	99.4 1.9 (10)	48.2 0.6 (4)	39.1 2.9 (2)	0.790 0.034	0.782 0.079
4	0	90.8 2.0 (10)	43.9 0.7 (4)	35.7 1.1 (2)	0.794 0.041	0.783 0.045
4	1	96.4 4.1 (10)	45.8 0.3 (4)	38.3 0.9 (2)	0.813 0.054	0.774 0.056
5	0	83.8 4.1 (10)	42.6 0.4 (4)	35.6 1.4 (2)	0.739 0.064	0.718 0.075
5	1	87.4 2.5 (10)	42.8 0.9 (4)	36.4 2.8 (2)	0.780 0.054	0.734 0.089
6	0	71.4 1.6 (10)	39.7 0.4 (4)	33.0 2.0 (2)	0.641 0.035	0.647 0.070
6	1	75.5 3.2 (10)	40.7 0.5 (4)	34.3 0.8 (2)	0.675 0.060	0.661 0.055
7	0	58.8 1.9 (8)	35.7 1.3 (4)	31.4 0.5 (2)	0.545 0.075	0.526 0.041
7	1	61.0 2.2 (8)	36.8 0.1 (4)	31.1 1.2 (2)	0.552 0.042	0.565 0.063
8	0	47.0 1.7 (8)	32.6 0.6 (4)	29.1 1.2 (2)	0.400 0.060	0.403 0.066
8	1	47.2 1.2 (8)	33.0 0.2 (4)	29.1 0.3 (2)	0.391 0.034	0.406 0.031
9	0	36.1 1.0 (6)	28.8 0.2 (4)	26.1 0.0 (2)	0.247 0.038	0.273 0.024
9	1	36.3 0.7 (6)	29.5 0.4 (4)	25.4 0.1 (2)	0.227 0.036	0.300 0.021
10	0	27.8 0.7 (6)	24.6 0.6 (4)	24.1 0.1 (2)	0.134 0.054	0.118 0.026
10	1	27.5 0.4 (6)	24.0 1.3 (4)	22.8 0.2 (2)	0.149 0.075	0.158 0.019
11	0	21.0 0.9 (6)	21.0 0.7 (3)	20.6 0.1 (2)	0.000 0.083	0.017 0.039
11	1	20.7 1.3 (6)	21.2 0.9 (4)	19.5 0.7 (2)	−0.026 0.115	0.049 0.084
12	0	14.8 0.5 (6)	18.0 0.4 (4)	17.2 0.8 (2)	−0.214 0.061	−0.126 0.067
12	1	15.3 0.8 (6)	17.1 0.4 (2)	17.7 0.2 (2)	−0.121 0.083	−0.124 0.055
13	0	12.2 0.6 (6)	15.1 1.0 (3)	15.4 0.1 (2)	−0.233 0.126	−0.196 0.048
13	1	12.1 0.8 (6)	14.7 0.0 (1)	15.4 0.1 (2)	−0.213 0.072	−0.203 0.062
14	0	9.4 0.6 (3)	11.5 0.3 (4)	12.9 0.3 (2)	−0.220 0.098	−0.263 0.071
14	1	9.4 0.4 (6)	11.7 0.2 (2)	12.9 0.3 (2)	−0.239 0.065	−0.263 0.053
15	0	8.0 0.8 (10)	9.4 0.3 (4)	10.9 0.3 (2)	−0.176 0.144	−0.262 0.110
15	1	8.0 0.8 (10)	9.4 0.4 (2)	10.9 0.3 (2)	−0.176 0.156	−0.262 0.110
16	0	6.8 0.4 (13)	7.6 0.0 (1)	9.6 0.3 (2)	−0.121 0.064	−0.288 0.075
16	1	6.8 0.4 (12)	7.5 0.5 (5)	9.6 0.3 (2)	−0.107 0.137	−0.288 0.075

The columns are the following: 1 and 2: identification of the transitions: the two true transitions associated with $|m|$ and k_0 are $|m|_{k_0,|m|} \leftrightarrow |m|-1_{k_0-1,|m|-1}$; for example $m=3$ $k_0=0$ corresponds to $3_{0,3} \leftarrow 2_{1,2}$ and $2_{1,2} \leftarrow 3_{0,3}$. (a) Room temperature air broadenings obtained (see text) using all available data. The three entries are the average half-width, the RMS, and the number of values used to calculate them. (b) Same as (a) but for 742 K. (c) Same as (a) but for 980 K. (d) Temperature exponent n_{742} and its uncertainty obtained from the 296 and 742 K data. (e) Temperature exponent n_{980} and its uncertainty obtained from the 296 and 980 K data.

data, two sets of temperature exponents n have been calculated using 296 K as a reference and the two other temperatures, i.e.

$$n_{742} = \ln[\gamma(296)/\gamma(742)]/\ln[296/742],$$
$$n_{980} = \ln[\gamma(296)/\gamma(980)]/\ln[296/980]. \quad (1)$$

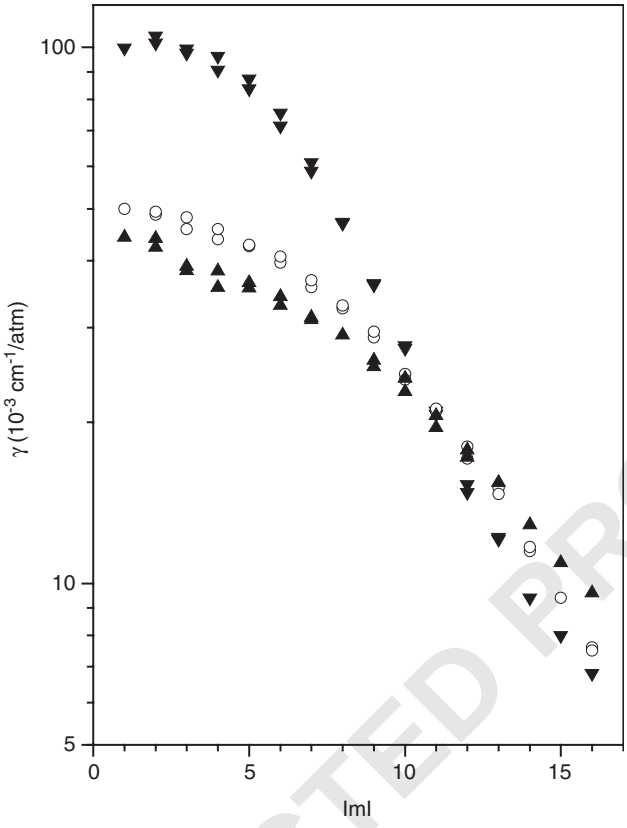

Fig. 2. Measured half-widths versus $|m|$ for the temperatures: ▼ 296 K, ○ 742 K, 980 K.

The associated uncertainties were calculated, *in a very pessimistic way*, by the relation

$$\Delta n_T = \frac{1}{2}\frac{\ln\{[\gamma(296)+\Delta\gamma(296)]/[\gamma(T)-\Delta\gamma(T)]\} - \ln\{[\gamma(296)-\Delta\gamma(296)]/[\gamma(T)+\Delta\gamma(T)]\}}{\ln[296/T]}. \quad (2)$$

The results are given in columns (d) and (e) of Table 3 and plotted in Fig. 3. They demonstrate the consistency of the measurements and confirm that n can be negative. Finally, the present values of $n = (n_{980} + n_{742})/2$ are compared with previous determinations [4,14] in significantly narrower temperature ranges (typically 240–296 K) in Fig. 4, showing that the present measurements agree with previous ones within experimental uncertainties.

4. Comparisons with calculations and discussion

4.1. Half-widths

N_2-broadening parameters have been calculated, for the mean relative thermal velocity $\bar{v}(T)$ only, using the model and data presented in Ref. [2]. These values, converted to air broadening

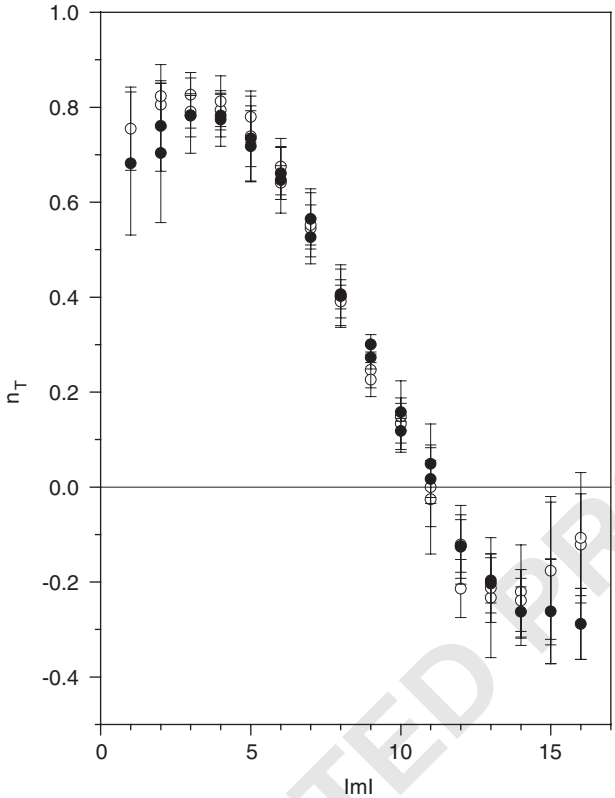

Fig. 3. Temperature exponents versus $|m|$ obtained from ○ 297/742 K and ● 297/980 K (see text).

(divided by 1.09) are compared with experimental determinations in Fig. 5. This shows that the model does predict a strong decrease of widths with $|m|$ but, as already noticed [2], the calculations increasingly overestimate the widths as $|m|$ increases. There are a number of possible and cumulative explanations for these discrepancies, which are discussed hereafter.

4.1.1. Effects of the potential

The first reason may be the intermolecular potential at short distances used. In order to check this possibility, we have varied the atom–atom parameters of the H_2O–N_2 interaction in order to improve the results at 296 K. The results, plotted in Fig. 6, show that accurate predictions can be obtained at room temperature but that the broadenings at elevated temperature are still overestimated (although slightly less than in Fig. 5).

4.1.2. Velocity dependence

Another explanation can be found in the use, for the calculations, of the mean relative thermal velocity only. Indeed, the negative temperature exponents observed (and calculated) indicate that the broadening cross sections $\sigma(v)$ strongly depend on v [$n = -0.3$ corresponds roughly to $\sigma(v) \propto v^{3/2}$]. In such cases of a strong dependence on the relative velocity, the widths predicted

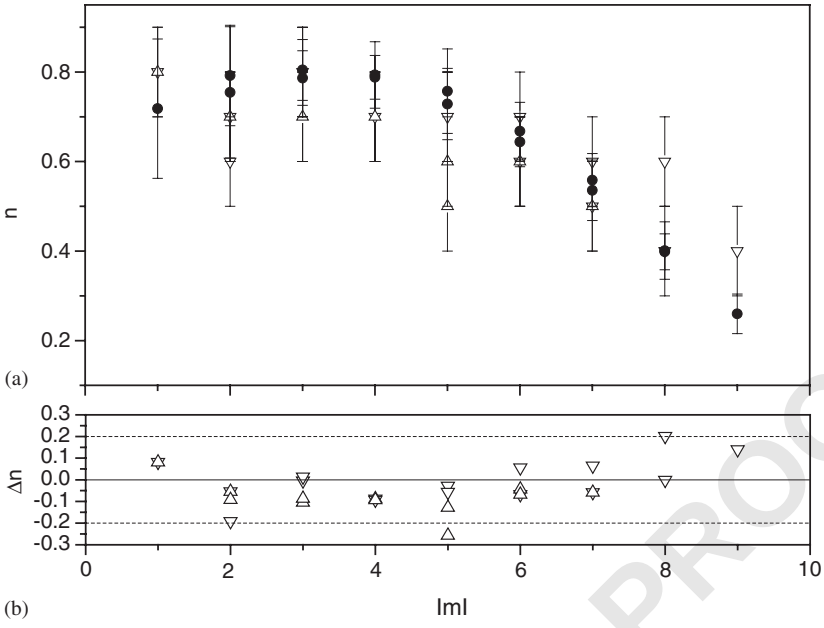

Fig. 4. Measured temperature exponents. (a) values of n from: • present work (average of n_{742} and n_{980}), ▽ Ref. [4], △ Ref. [14]. (b) absolute differences between the present determinations of n and the values from ▽ Ref. [4], △ Ref. [14].

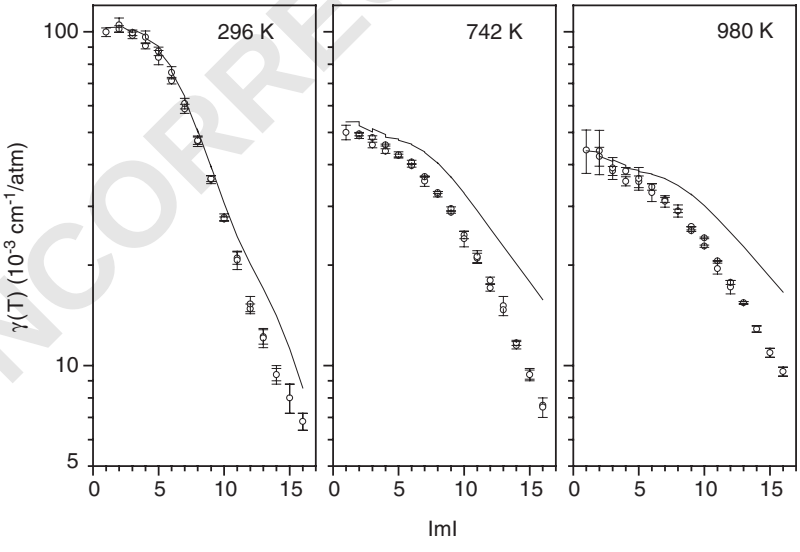

Fig. 5. Comparisons between measured (○) widths and values (—) calculated for the mean relative velocity (with the potential of Ref. [2]) at the three temperatures.

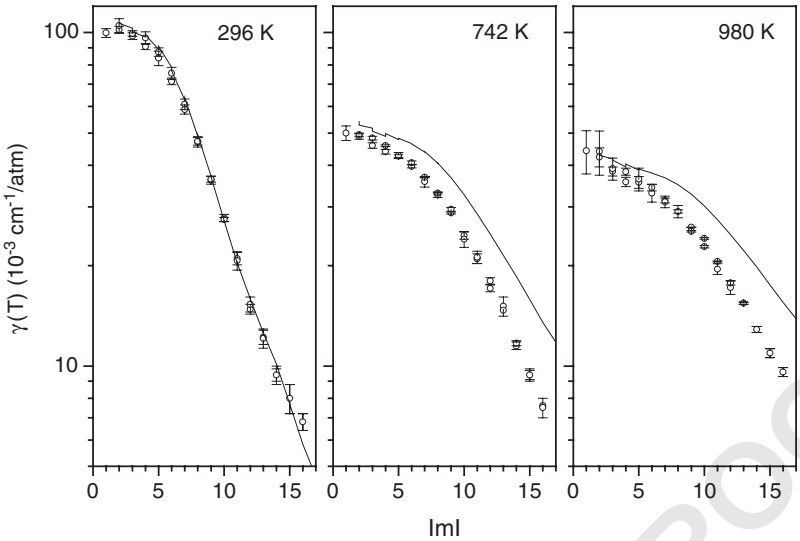

Fig. 6. Same as Fig. 5 but calculations have been made with atom–atom potential parameters modified in order to obtain agreement at 296 K.

from the mean velocity, i.e.

$$\gamma[\bar{v}(T)] \equiv \bar{v}(T) \times \sigma[\bar{v}(T)], \tag{3}$$

can be very different from the velocity averaged value:

$$\bar{\gamma}(T) \equiv \int_0^{+\infty} v \times \sigma(v) \times f_{\mathrm{MB}}(v, T)\,\mathrm{d}v, \tag{4}$$

where f_{MB} is the Boltzmann distribution.[2]Comparisons between calculated values of these two widths are plotted in Fig. 7 showing that the velocity averaging mostly affects the broadenings of narrow lines at low temperature. This can be understood looking at the typical results in Fig. 8, which are qualitatively similar to what is predicted by both semi-classical and close-coupling calculations for other light molecules such as HF [21,22] and HCl [23]. This figure shows that, for low J lines, which mostly involve small rotational energy transfers, $\gamma(v)$ nicely verifies a $v^{2/3}$ dependence. In this case, $\sigma(v) \propto v^{-1/3}$ and$\gamma[\bar{v}(T)]$ is slightly smaller than $\bar{\gamma}(T)$.[3]For high J transitions, the situation is very different since their broadening is due to rotational transfers $r' \leftarrow r$ that involve large energy jumps $|\Delta E_{r'r}|$. In this case, collisions with small relative velocities are very non-resonant and thus inefficient (recall that the *resonance functions* decrease quickly and depend on quantities proportional to $|\Delta E_{r'r}|/v$ [24,25]). Hence, for high J lines, starting from very inefficient collisions—i.e. small values of $\sigma(v)$—at low v, collisions become more and more efficient

[2]In fact, one can analytically show from Eqs. (3) and (4) that $\bar{\gamma} = \gamma(\bar{v})$ is $\sigma(v)$ is independent of v or proportional to $1/v$ but that, when $\sigma(v)$ is proportional to v or to v^2 one has $\bar{\gamma} = 3\pi\gamma(\bar{v})/8 \approx 1.1\gamma(\bar{v})$ or $\bar{\gamma} = \pi\gamma(\bar{v})/2 \approx 1.6\gamma(\bar{v})$, respectively.

[3]For resonant collisions involving a single potential term in R^{-n}, $\sigma(v)$ and $\gamma(v)$ are proportional to $v^{-2/(n-1)}$ and $v^{(n-3)/(n-1)}$, respectively. For a dipole–quadrupole interaction ($n = 4$). $\sigma(v)$ is thus proportional to $v^{-2/3}$. For $\sigma(v)$ proportional to $v^{-1/3}$, numerical calculations show that $\bar{\gamma} \approx 0.98\gamma(\bar{v})$.

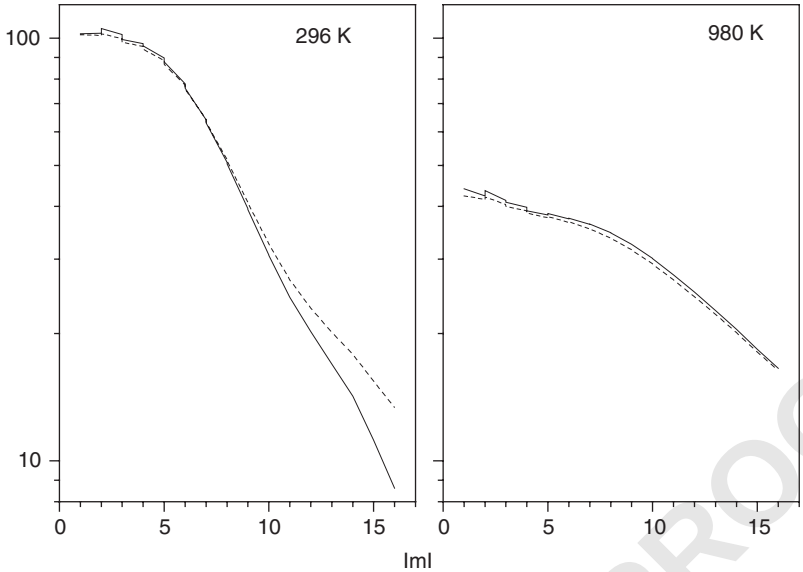

Fig. 7. Effect of velocity averaging at two temperatures. — $\gamma[\bar{v}(T)]$, - - - $\bar{\gamma}(T)$.

as resonance is progressively overtaken [5] as $|\Delta E_{r'r}|/v$ decreases with the increase of v. For the $16_{1,16} \leftarrow 15_{0,15}$ transition at low temperatures, $\bar{\gamma}(T)$ results mostly from the strongly increasing values of $\gamma(v)$ at low velocities—$\sigma(v)$ varies as $\approx v^{2.5}$ for v between 500 and 1000 m/s, see Fig. 8—, and is thus significantly larger than $\gamma[\bar{v}(T)]$.[2] At elevated temperature, where the Boltzmann distribution spreads towards higher velocities, $\bar{\gamma}(T)$ results mostly from the slowly increasing values of $\gamma(v)$ at large v-values—$\sigma(v)$ varies as $\approx v^{0.2}$ for v above 1500 m/s, see Fig. 8—, and is thus close to $\gamma[\bar{v}(T)]$.

It is important to recall that, when the dependence of $\sigma(v)$ on v is strong, neither $\bar{\gamma}(T)$ nor $\gamma[\bar{v}(T)]$ can be directly related with experimental values since the measured profile does not depend on these quantities. Indeed, in this case, it is the spectral shape itself that has to be averaged (e.g. [26–28] and references therein) over the distribution of the H_2O absolute velocities v_{H_2O} with collisional parameters that are averaged over the perturber absolute velocities v_{N_2}. In the simple case where Doppler effects, speed changing collisions, and correlations are negligible this leads to a weighted sum (over v_{H_2O}) of Lorentzian profiles. The spectral shape can then be significantly non-Lorentzian and the question "what calculated quantity is to be compared with measured widths?" is crucial. Although there is no direct answer to this problem, the best way would probably be to simulate the profile under the exact pressure–temperature experimental conditions using calculated values of $\gamma(v)$ and then to fit it with the same procedure as that which is used to treat the measured spectrum. This problem, which is out of the scope of the present paper, will be the subject of a future work (see footnote 1).

4.1.3. Semi-classical model

A final possible explanation for the results obtained here may be found in the use of a semi-classical model. Indeed, such an approach, which neglects exchanges between rotation and

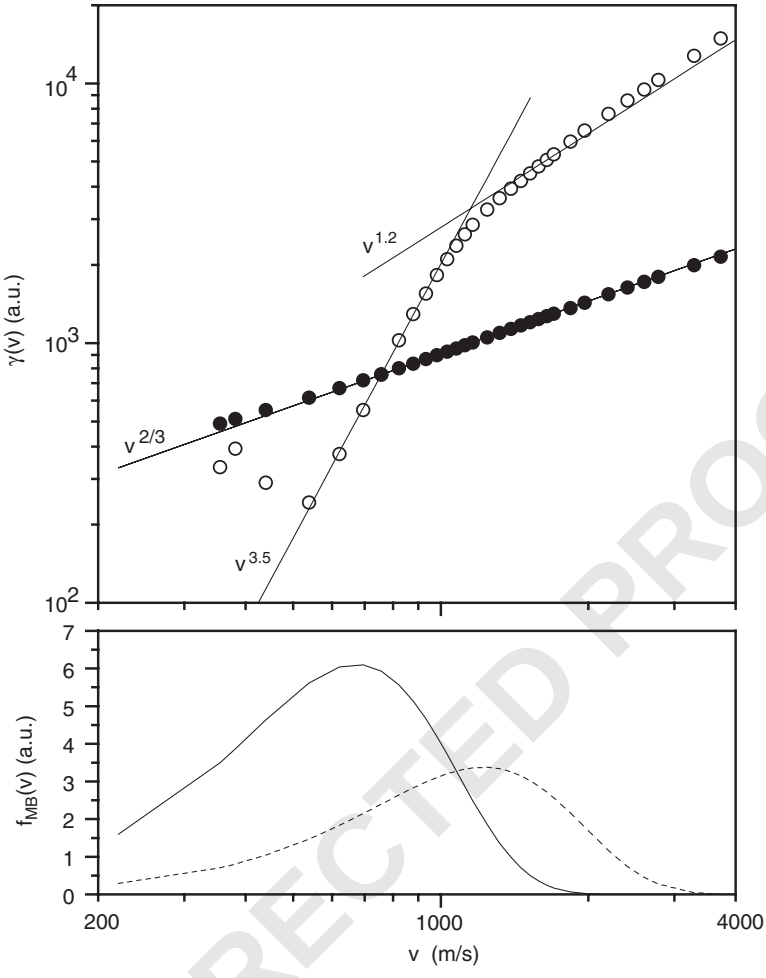

Fig. 8. Velocity dependences. In the top panel are plotted typical variations of $\gamma(v)$ for the $4_{1,4} \leftarrow 3_{0,3}$ (•) and $16_{1,16} \leftarrow 15_{0,15}$ (○) lines. The Boltzmann distributions at 296 K (—) and 980 K (- - -) are displayed in the lower panel.

translation, is valid, strictly speaking, only when rotational energy jumps induced by collisions are small when compared to the kinetic energy (i.e., $\approx kT$). Although the quantitative limit of validity is unknown, calculations for high J lines may be affected by the use of a classical path approach.

4.2. Temperature dependence

As mentioned above, the question of what calculated quantity is to be compared with measured values is a complex problem when velocity effects are strong (high J lines) since neither $\bar{\gamma}(T)$ nor $\gamma[\bar{v}(T)]$ but some more complex average value should be used. Nevertheless, for comparison with experiments, we have calculated the temperature exponents n_T from calculated values of both $\bar{\gamma}(T)$ and $\gamma[\bar{v}(T)]$ using Eq. (1). The averages $n = (n_{742} + n_{980})/2$ are compared with the corresponding experimental determinations in Fig. 9. This shows that the calculations do predict

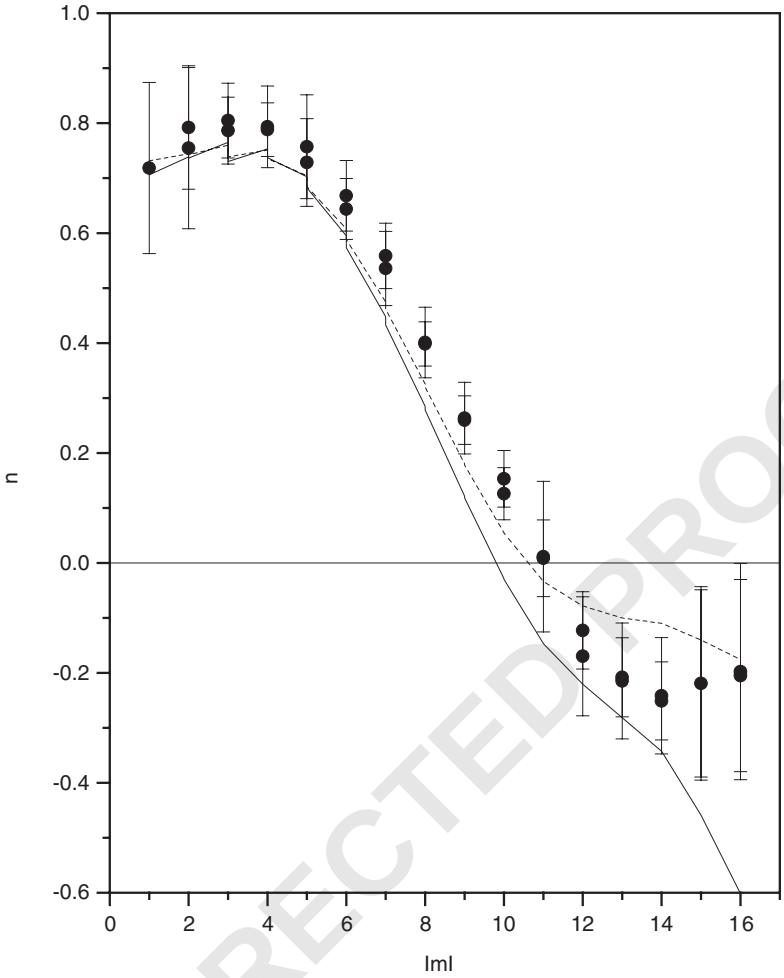

Fig. 9. Comparisons between measured values of the average temperature-dependence coefficient $n = (n_{742} + n_{980})/2$, and those obtained from calculations of — $\gamma[\bar{v}(T)]$ - - - $\bar{\gamma}(T)$.

the strong decrease of n with J and the negative values for transitions involving high rotational energy. Furthermore, although there is no theoretical justification for this as mentioned above, quantitative satisfactory agreement is obtained between experiments and calculations when the averaging of $\gamma(v)$ is made. It is worth noting that this result and those plotted in Figs. 5–7 suggest that correct predictions of both $\gamma(T)$ and n could likely be obtained by adjusting the interaction potential at short distances in calculations where the averaging over v is made.

5. Conclusion

The present work shows that the evolutions of H_2O collisional-broadening parameters with temperature show large variations from line to line. It also brings the experimental confirmation,

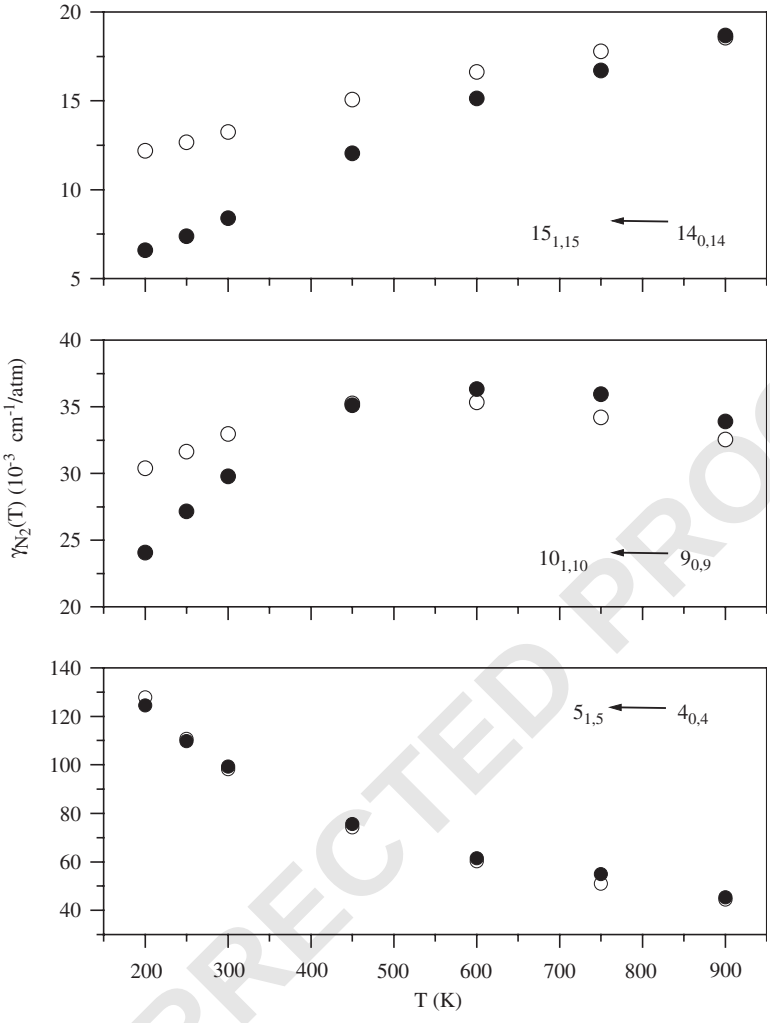

Fig. 10. N_2-broadening coefficients of three H_2O ν_2 doublets obtained from calculations of • $\gamma[\bar{v}(T)]$, ○ $\bar{\gamma}(T)$.

to our knowledge for the first time, that the widths of transitions involving large rotational energies can increase with T. This result is due to the strong increase of the corresponding broadening cross sections $\sigma(v)$ with the relative velocity v between the active molecule and the collision partner. Theoretical calculations with a semi-classical model confirm the large range of temperature exponents n that vary from typically +0.8 down to −0.3 from low-to-high J transitions. The analysis suggests that good agreement between experiments and predictions for both $\gamma(T)$ and n could be obtained, provided that the average over the velocity distribution is performed and that the interaction potential is adjusted. Nevertheless, the strong variations of $\sigma(v)$ call for a refined study of the (inhomogeneous) effects of velocity averaging on the spectral shape itself for an extended pressure range from the Doppler to the collisional regime. Furthermore, experimental studies of doublet lines from low-to-high J for a refined temperature

grid in a wide range of T would be of considerable interest. Indeed, the values in Fig. 8 indicate that significant deviations from the temperature power law should be observed, as further illustrated by Fig. 10. Experimental confirmation of this prediction is a study that deserves attention.

Acknowledgements

R.R. Gamache is pleased to acknowledge support of this research by the National Science Foundation through Grant No. ATM-0242537. Any opinions, findings, and conclusions or recommendations expressed in this material are those of the author(s) and do not necessarily reflect the views of the National Science Foundation. G. Wagner and M. Birk wish to thank the Commission of the European Communities for funding through contracts BRPR-CT96-0142 and BRPR-CT97-0509.

References

[1] Gamache RR, Hartmann JM, Rosenmann L. Collisional broadening of water–vapor lines: I. A survey of experimental results. J Quant Spectrosc Radiat Transfer 1994;52:481–99.
[2] Gamache RR, Hartmann JM. Collisional parameters of H_2O lines: effects of vibration. J Quant Spectrosc Radiat Transfer 2004;83:119–47.
[3] Gamache RR, Hartmann JM. An intercomparison of measured pressure-broadening and pressure-shifting parameters of water vapor. Can J Chem, submitted for publication.
[4] Zou Q, Varanasi P. Laboratory measurement of the spectroscopic line parameters of water vapor in the 950–2100 and 3000–4050 cm^{-1} regions at lower-tropospheric temperatures. J Quant Spectrosc Radiat Transfer 2003;82:45–98.
[5] Hartmann JM, Taine J, Bonamy J, Labani B, Robert D. Collisional broadening of rotation-vibration lines for asymmetric-top molecules. II. H_2O diode laser measurements in the 400–900 K range; calculations in the 300–2000 K range. J Chem Phys 1987;86:144–56.
[6] Lynch R, Gamache RR, Neshyba SP. Fully complex implementation of the Robert–Bonamy formalism: halfwidths and line shifts of H_2O broadened by N_2. J Chem Phys 1996;105:5711–21.
[7] Gamache RR, Lynch R, Neshyba SP. New developments in the theory of pressure-broadening and pressure-shifting of spectral lines of H_2O: the complex Robert–Bonamy formalism. J Quant Spectrosc Radiat Transfer 1998;59:319–35.
[8] Claveau C, Henry A, Hurtmans D, Valentin A. Narrowing and broadening parameters of H_2O lines perturbed by He, Ne, Ar, Kr and nitrogen in the spectral range 1850–2140 cm^{-1}. J Quant Spectrosc Radiat Transfer 2001;68:273–98.
[9] Claveau C, Henry A, Lepère M, Valentin A, Hurtmans D. Narrowing and broadening parameters for H_2O lines in the ν_2 band perturbed by nitrogen from Fourier transform and tunable diode laser spectroscopy. J Mol Spectrosc 2002;212:171–85.
[10] Non-Intrusive Measurement of Aircraft Engine Exhaust Emissions (AEROJET). Final technical report, Commission of the European Communities Contract No. BRPR-CT96-0142, 1998.
[11] Lindermeir E, editor. AEROPROFILE: profiling spectrometry to simultaneously investigate the spatial distribution of temperature and chemical species in aircraft exhausts. Report to BRITE-EURAM Project No. BE97—4467, Contract No. BRPR-CT97-0509, DLR.

[12] Schäfer K, Heland J, Lister DH, Wilson CW, Howes RJ, Falk RS, Lindermeir E, Birk M, Wagner G, Haschberger P, et al. Nonintrusive optical measurements of aircraft engine exhaust emissions and comparison with standard intrusive techniques. Appl Opt 2000;39:441–55.
[13] Wagner G, Birk M, Schreier F, Flaud J-M. Spectroscopic database for ozone in the fundamental spectral regions. J Geophys Res 2002;107:4626.
[14] Remedios JJ. Spectroscopy for remote sensing of the atmosphere. Phd, University of Oxford, 1990.
[15] Toth RA, Brown LR, Plymate C. Self-broadened widths and frequency shifts of water vapor lines between 590 and 2400 cm^{-1}. J Quant Spectrosc Radiat Transfer 1998;59:529–62.
[16] Labani B, Bonamy J, Robert D, Hartmann JM. Collisional broadening of rotation-vibration lines for asymmetric-top molecules. III. Self-broadening case: application to H_2O. J Chem Phys 1987;87:2781–9.
[17] Rothman LS, Rinsland CP, Goldman A, Massie ST, Edwards DP, Flaud JM, Perrin A, Dana A, Mandin JY, Schroeder J, McCann A, Gamache RR, Wattson RB, Yoshino K, Chance KV, Jucks KW, Brown LR, Nemtchinov V, Varanasi P. The HITRAN molecular spectroscopic database and HAWKS (HITRAN atmospheric workstation): 1996 edition. J Quant Spectrosc Radiat Transfer 1998;60:665–710.
[18] Toth RA. Air- and N_2-broadening parameters of water vapor: 604 to 2271 cm^{-1}. J Mol Spectrosc 2000;201:218–43.
[19] Nicolaisen FM. ASA workshop paper 5.8, Moscow, June 6–8, 1990.
[20] Yamada KMT, Harter M, Giesen T. Survey study of air-broadened water vapor lines in the ν_2 band by high-resolution FTIR spectroscopy. J Mol Spectrosc 1993;157:84–94.
[21] Hartmann JM, Boulet C. Line shape parameters for HF in a bath of argon as a test of classical path models. J Chem Phys 2000;113:9000–10.
[22] Green S, Hutson J. Spectral line shape parameters for HF in a bath of Ar are accurately predicted by a potential inferred from spectra of the Van Der Waals dimer. J Chem Phys 1994;100:891–8.
[23] Roche CF, Hutson JM, Dickinson AS. Calculations of line width and shift cross sections for HCl in Ar. J Quant Spectrosc Radiat Transfer 1995;53:153–64.
[24] Tsao CJ, Curnutte B. Line-widths of pressure-broadened spectral lines. J Quant Spectrosc Radiat Transfer 1962;2:41–91.
[25] Robert D, Bonamy J. Short range forces effects in semi classical molecular line broadening calculations. J Phys (Paris) 1979;40:923–43.
[26] Robert D, Lance B. Correlation effect in spectral line shape from the Doppler to the collision regime. J Chem Phys 1999;111:789–92.
[27] Chaussard F, Michaut X, Berger H, Joubert P, Lance B, Bonamy J, Robert D. Collisional effects on spectral line shape from the Doppler to the collisional regime: a rigorous test of an unified approach. J Chem Phys 2000;112:158–66.
[28] Chaussard F, Saint-Loup R, Berger H, Joubert P, Bruet X, Bonamy J, Robert D. Speed-dependent line profile: a test of a unified model from the Doppler to the collisional regime for molecule–molecule collisions. J Chem Phys 2000;113:4951–6.